Wang, Y., Chea, M. K., Belnoue, J. P., Kratz, J., Ivanov, D., & Hallett, S. R. (2020). Experimental characterisation of the in-plane shear behaviour of UD thermoset prepregs under processing conditions. *Composites Part A: Applied Science and Manufacturing*, *133*, [105865]. https://doi.org/10.1016/j.compositesa.2020.105865

Experimental characterisation of the in-plane shear behaviour of UD thermoset prepregs under processing conditions

Yi Wang[1*], Ming Kai Chea[1,2], Jonathan P.-H. Belnoue[1], James Kratz[1], Dmitry S. Ivanov[1]and Stephen R. Hallett[1]

[1]Bristol Composites Institute (ACCIS), University of Bristol, UK

[2]School of Engineering Sciences, KTH Royal Institute of Technology

*Corresponding Author: Yi.Wang@bristol.ac.uk

Abstract

The in-plane shear behaviour of an uncured composite material (i.e. prepreg sheet, dry fibre preforms etc) is one of the key parameters that influences wrinkles generation in advanced composites manufacturing processes such as automated fibre placement (AFP) and thermoforming. However, there is no standardised test method for the characterisation of uncured unidirectional prepreg subjected to pure shear loading. In this paper, a 10° off-axis tensile test is developed, and the method's suitability is demonstrated on two different materials. The mechanical response is analysed over a range of testing rates and temperatures that are consistent with the real manufacturing process parameters. The results demonstrate the feasibility of the test method for extracting relevant material characteristics and the strain-rate and temperature dependency of the material response.

Keywords: A. Prepreg; B. Rheological properties; D. Mechanical testing; E. Prepreg Processing

1. Introduction

Current fast-growing demand and large-scale usage of advanced composites in the aerospace, automotive and renewable energy sectors have intensified the need for more efficient and cheaper manufacturing techniques. Automated fibre layup (AFP), which can greatly improve productivity and also help reduce material wastage inherent to the fabrication of composite structures, has been a key enabler of this recent push for productivity, especially in the aerospace industry. The likelihood of process-induced defects such as wrinkles limits the applicability to complex geometries, especially when curved fibre trajectories are required. When the material is deposited on a curved surface or steered along a curved path, the mismatches between the deformation of the inner (in compression) and outer (in tension) radii can lead to the formation of fibre path defects [1]. This material behaviour is dictated by the ratio of the shear to the bending stiffness for single ply forming whilst inter-ply friction also plays a major role in multi-ply forming. Similar phenomena also occur in thermoforming - one of the preferred manufacturing methods in the automobile sector where compliant thin sheets of material are conformed to complex-shaped moulds (e.g. doubly curved surface), which induces significant shear deformation that, in

turn, lead to the formation of wrinkles. As these defects will cause a significant loss of the in-service product's performance, they must be minimised or fully avoided [1]. This is traditionally dealt with through expensive and time-consuming trial-and-error experimental programs that considerably impact the economics, i.e. 70% of the cost of manufacturing a composite part is typically spent before a single defect-free part has even been manufactured, Poursatip [2] quotes an example of this from the aerospace sector. Being able to replace many of these initial trials by numerical process simulations could help to drastically reduce the cost of new part development. Textile forming is generally well understood, especially for dry fabrics [3,4]. The methods to simulate dry preforms have been successfully adapted to simulate draping of textile prepregs [5,6]. However, applications of forming of unidirectional (UD) prepregs are limited to thermoplastics [5] and the literature on modelling and characterisation of UD thermoset prepreg is quite sparse. This is well illustrated by the current advancement in the field of the modelling of AFP processes that is mostly dominated by simple analytical approaches [7–9] with very few example of FE-based numerical simulations [10,11] as the lack of adequate constitutive models for the tape makes their relevance questionable.

The examples above highlight the key role played by in-plane shear in the defect formation mechanisms in composite manufacturing. It can also be found in the open literature on thermoforming [3,5,12,13], AFP deposition [7–9,11], and autoclave curing processes [14–16]. These works indicate the highly temperature and rate dependent nature of prepreg loaded in pure shear, which will manifest itself in the real manufacturing processes and needs to be considered in any virtual platform aiming at simulating them. For dry or impregnated biaxial fabrics, the picture frame shear test [17–19] and the bias extension test [19–21] have become the preferred testing methods for the characterisation of the in-plane shear behaviour. However, these methods are not suitable for UD prepregs, the material form that allows manufacture of composite structures with the very best quality and highest mechanical properties. Prepregs are thin, extremely compliant and hard to handle. It is difficult to devise a testing procedure where a pure deformation mode can be guaranteed, where samples do not buckle out-of-plane and where they keep their integrity until advanced deformation stages. There are extra complications induced by the fact that the experimental procedure should allow testing at different loading rates and temperatures due to the presence of uncured resin in the material. The dependence of the measured mechanical response on specimen size, as observed for prepreg consolidation [14,15] and shear of engineering fabrics [4], should also be investigated.

There have numerous attempts to address the challenge of in-plane shear testing for UD prepregs. In particular, Scobbo and Nakajima [22] and, later, Stanley and Mallon [23] proposed similar fixtures consisting of three parallel plates. The top and bottom plates were fixed, while the central plate could be pulled-out dynamically. Consolidated unidirectional laminates were placed against both sides of the

central plate and the dynamic shear deformation was induced by oscillating translational motion of the central plate [22] or pulling-out the plate at a constant velocity to obtain a steady-state shear deformation [23]. The test shows some clear trends in material behaviour. The main difficulty of the test is that the loading direction parallel to the fibres may inevitably result in the localisation of the deformation in resin rich area at the fixture-specimen interface as well as in between the plies. It is also not clear whether inter-ply sliding contributes to the deformation mechanism. Similar problems apply to the test method proposed by Groves [24,25] who introduced a test set-up where UD thermoplastic laminates were placed between two parallel rheometer platens. The test was later adapted by Hormann [10] for the testing of thermoset-based prepreg. In this test, shear deformation is induced by rotating one of the plates and the laminates can be made of either off-centre UD or cross-ply layups that are sheared under low frequency oscillatory motion. There is a challenge in interpreting the test results and translating them to a model due to non-uniform deformation distribution along radial coordinates.

Other methodologies trialled to characterise the in-plane shear behaviour of UD prepreg include those that consists of adapting standardised methods for fabric such as the bias extension [26] and the picture frame [17] tests. The main issue with these methods is that, in order to compensate for the unidirectionality of the fibres, testing is performed on cross-ply laminates bringing, once more, the question disambiguating in-plane and inter-ply shear response. This was corroborated by Larberg et al. [26] who performed bias extension tests on various cross-plied unidirectional prepregs at ±45 and showed that in-plane shear only dominates at small deformations. The picture frame shear test also brings more specific problems such as the difficulty to achieve a uniform temperature field over the large sample and the propensity for ply splitting and adverse fibre tension under the combined effect of slight fibre misalignment and the tight clamping of the sample in the frame.

Recognising the challenges of the different tests mentioned above, Haanappel and Akkerman [27], more recently proposed a torsion bar test. The test's setup consisted of a rheometer and a standard torsion fixture making it easy to implement. Thick unidirectional prismatic specimens manufactured from 80 plies of AS4/PEEK were twisted by oscillating rotations in a controlled environment. The kinematics of the test was analytically derived to separate the shear and axial contributions to the measured applied load. The test was later adopted by Dörr et al. [12] for intra-ply shear characterisation for UD-PA6-CF. Single transient loads were applied and material parameters were extracted through an inverse Finite Element (FE)-based method. Although the test procedure helped to gain valuable insights into the complex rheological behaviour of fibre reinforced melts under shear loading (e.g. the elastic contribution of fibres to the overall response which, for a long time, had been considered to be negligible [28,29]), it may be difficult to adopt as a standardised shear test for UD prepreg as high frequencies are only possible in the small strain regime. In contrast, large strain torsion bar testing is restricted to moderate strain rates.

The relatively thick samples with close to square cross-sections are time-consuming to manufacture, which also limits the possibility to perform a thorough experimental campaign with enough repeats and variation of testing parameters. Lastly, the 'thin' sheet conditions of the prepreg during the forming process cannot be reproduced.

Exploring the deformation processes within UD prepreg, Potter [30] conducted an initial attempt for in-plane deformation characterisation by an off-axis tensile test. Strips of prepreg with a fibre angle varying between 90^{o} and 15^{o} were laid up and subjected to tensile loading under room temperature. The shear angle was obtained by marking lines on the samples and tracking the change using a series of video images captured during the test. It was shown that the deformation was dominated by transverse stretching for off-axis angle 90° to 30°, whilst shear became dominant at an off-axis angle of 15°. The tests pointed out the possibility to obtain the in-plane shear information of prepreg by off-axis testing and the necessity of more sensitive measurement methods for the strain field. A similar test was subsequently tried by Schirmaier et al. [31] to obtain the evolution of spatial distribution of the in-plane strain components on unidirectional non-crimp fabrics (UD-NCF) subjected to multi-axial deformation.

Characterisation methods of UD prepregs' in-plane shear behaviour typically reported in the literature mostly focus on thermoplastic-based systems rather than thermosets and strain rates achieved were between 0.0016 s^{-1} to 10 s^{-1} for thermoplastics and 0.0008 s^{-1} to 0.004 s^{-1} for thermosets [10]. The present contribution proposes an adaptation of Potter's [30] off-axis tensile test to characterise the in-plane shear behaviour of toughed UD thermoset prepregs. As described at length in section 2.2, this test is characterised by the existence of a highly strained region at the centre of the specimen that is populated with fibres that are not clamped at either end. The size of this region can be adjusted by changing the dimensions of the samples and the relative amount of shear and transverse stretching (that coexist) can be controlled by varying the angle of the fibres from the main loading direction. As opposed to the original paper on off-axis test [30] that mostly focused in exploring how different ratios of shear and transverse stretching affects the integrity of the fibrous sheets, in this paper, the fibres were oriented at 10^{o} in order to maximize the amount of shear generated in the samples. Digital Image Correlation (DIC) was used to measure the strains generated in the area where deformation localises and (shear) stresses were also resolved locally in the band thus allowing the extraction of the material laws controlling the behaviour of the material under (almost) pure shear. The proposed method has the advantage of providing direct measurements of the strains and a simple way to obtain the stresses, that avoids complex or inverse procedures. The mathematical form of the material constitutive relation does not therefore have to be assumed a-priori. The possible influence of the extensional viscosity transverse to the fibres is separated from the global response in the data extraction procedure and the energy dissipated through extension in

the direction of the fibres is neglected as it is well accepted that η_{11} is much smaller than η_{22} (see Batchelor [32] and Pipes [33]). The measured ε_{11} and ε_{22} are well below ε_{12}, as shown in Figure 2 b/. The stresses in the region of interest can thus be resolved into shear (plus a negligible extensional component along the fibre direction) and transverse extension components. The shear response of the prepreg is obtained by plotting the resulting shear stress as a function of the shear strain, which is directly measured through DIC.

In the first part of the paper, the feasibility of the test method was evaluated and the influence of a range of process parameters relevant to the AFP deposition process (namely specimen dimensions and loading rate) were studied. This initial test campaign allowed to reduce the test matrix of subsequent tests where a more systematic study of the influence of temperature, loading rate and material type was performed. This is presented in the second part of the paper. Three different strain rates (i.e. 0.001 s^{-1} /0.01 s^{-1} /0.1 s^{-1}) and temperatures (i.e. 25ºC, 50ºC and 75ºC) and two aerospace-grade commercial thermoset prepregs (namely IM7/8552 [34] and IMA/M21 [35], see Table 1) were tested. All possible combinations between these test parameters were studied. The differences in the micro- and meso-scale morphology of the two materials were used to explain the features in their measured shear behaviour. The proposed test method also allows to reach deformation speeds that are much closer to those seen in automated manufacturing processes such as AFP (where the maximum possible shear rate is between 0.2 s^{-1} to 0.5 s^{-1} as shown in section 2.1) and thermoforming (where the deformation rate is typical from 0.1 s^{-1} to 10 s^{-1} [36]) compared to methods proposed in the past [10].

2. UD prepreg in-plane shear characterisation through 10° off-axis test

2.1 Upper bound estimation of the maximum shear rate in the AFP deposition process

Previous experimental programmes for characterisation of shear in UD thermoset prepreg have mostly explored strain rates between 0.0008 s^{-1} to 0.004 s^{-1} [10] which is very low in comparison to the shear rates applied to the material in real industrial processes. To determine the range of shear rate that should ideally be covered, an estimation of the shear rates applied to prepreg tapes during the AFP deposition process was made. This estimation aims at an upper bound analysis, where it is assumed that a prepreg tape can only shear when steered by an AFP roller and uses the layup speed of an AFP machine reported in the literature [1]. In reality the process involves both bending and shear deformations of the tape.

The path of the tape is described by the geometry and position of its neutral axis, and its shear angle is denoted by γ, as shown in Fig. 1. l and w are the length and width of the tape, respectively. r is the radius of the inner curvature and α is the corresponding rotation angle. Assuming that the roller is steered at a speed v over time Δt, the combination of geometrical relationships and of the definition of the shear rate allow to derive Eq. (1) and (2) as:

$$\gamma \approx \tan\gamma = \frac{\Delta l}{h} = \frac{(r+w)\cdot\alpha - \left(r+\frac{w}{2}\right)\cdot\alpha}{\frac{w}{2}} = \alpha \quad (1)$$

$$\dot{\gamma} = \frac{\Delta\gamma}{\Delta t} = \frac{\Delta\alpha}{\Delta t} = \frac{\Delta l}{r\cdot\Delta t} = \frac{v}{r} \quad (2)$$

The maximum layup speed of an AFP machine typically reported in the literature is 1 m/s [1]. However, in order to achieve better deposition quality, the machines are often programmed to be slower for curved paths, and this can decrease even further for the deposition on a non-flat geometry due to the constraints imposed by the robotic movements. For a steering radius of 900 mm the layup speed will typically decrease to around 200-500 mm/s giving sufficient time for the machine to accelerate. To avoid steering defects, it is usually preferable for the steering radius to not be below 500 mm. Feeding this into Eq. (2), the maximum shear rate seen by the tape can be estimated to be between 0.22 s^{-1} (for a layup speed of 200 $mm{\cdot}s^{-1}$) and 0.56 s^{-1} (for a layup speed of 500 $mm{\cdot}s^{-1}$). This is about 2 orders of magnitude higher than the maximum test rates studied in the past. It should also be noted that a lower bound analysis, where it is assumed that the deformation of tapes under is solely due to bending, estimates the shear rate to be 0 s^{-1}.

2.2 Overview of the off-axis test method

As mentioned in the introduction, many different tests for the characterisation of shear in dry fabrics and resin melts reinforced with fibres have been proposed over the years. All of them have advantages and disadvantages. The off-axis test method inspired by Potter [30] was used in this paper. Whilst the smallest angle used by Potter was 15°, the indication from trial test results was that 10° has a larger measured force than that of 15°. Therefore, the decision was taken to use a 10° angle in order to have higher resolution of the measured value, especially at high temperature where the material is more compliant. As mentioned in introduction, another benefit of this was to increase the amount of shear deformation generated in the sample. Hence, as documented in the original paper by Potter [30], the deformation within the sample can be very complex with a mix between pure shear and small local transverse extension in the localisation area and also some lengthening of the specimen side length outside the 'highly sheared region' together with a change in fibre angle away from the loading direction. At low fibre angles however, deformation is entirely contained in the localisation area and the different deformation modes can be separated as described below.

A particularity of the off-axis test method, which is often seen as a disadvantage, is the non-uniformity of the strain field it produces over the entire sample surface. Various of deformation (longitudinal tension/transverse tension/shear) occurs within the whole specimen. In the paper, a shear band area was designed, as shown in Fig. 2 a/, and the study focuses on the local state in the band. The geometry of the test is, indeed, such that some of the fibres are not clamped on both ends. Application of

a tensile load results in the creation of a highly sheared region in the middle of the sample. Fig. 2 b/ shows the strain fields ($\varepsilon_{11}/\varepsilon_{12}/\varepsilon_{22}$ in the fibre local coordinate system) in a specimen during testing. This was obtained through DIC. It can be seen that a highly sheared region is created and there is almost no other deformation out of the band. The size of this shear band can be controlled by the geometry of the sample and this is used to advantage here to create a test which is especially relevant to AFP processes. By setting the dimensions of the sample in a way that the width of the sheared region corresponds to the width of an AFP tape, possible size effects [14] are studied by adjusting the width of the shear zone to different pre-determined values and comparing the mechanical behaviours obtained.

A schematic of the test geometry and stress state in the highly strained region of the tape is shown in Fig. 2. θ is the off-axis angle and coordinates x-y and 1-2 are the overall and local coordinate systems respectively, with the force being applied in the x direction, and the local axis 1 marking the direction of the fibres. *F* is the applied force and A the cross-section area of the samples (which is obtained by multiplying sample thickness and width). Rotating the applied stress state in the global coordinate system to local coordinates allows expression of the local normal stress (σ_{11}), the local normal stress in transverse direction (σ_{22}) and local shear stress (τ_{12}) respectively, as Eq. (3). These equations are applicable for stress tensor calculations in small strain. For large deformation, corrections need to be made from engineering stress to true stress, and the geometric nonlinearity arising from the fibres' rotation during the test needs to be accounted for. This leads to the relation:

$$\sigma_{11} = \frac{F \cdot \cos^2\theta}{A}, \quad \sigma_{22} = \frac{F \cdot \sin^2\theta}{A}, \quad \tau_{12} = \frac{F \cdot \sin 2\theta}{2A} \tag{3}$$

It is important to note here that these equations have been used to calculate stresses within the localisation area assuming that there is only a very small amount of deformation outside it.

The geometrical relationship within the sample is given in Eq. (4). w and w_b are the width of the sample and shear band, respectively while l and l_g are the total length of the sample and the length of the grip area.

$$l = \frac{w}{\tan\theta} + \frac{w_b}{\sin\theta} + l_g \tag{4}$$

As illustrated Fig. 2, the localised highly deformed area is subjected to both shear and transverse tension stresses. The magnitude of transverse tensile deformation was shown to be very small under 15° off-axis loading [30] and DIC measurements on a 10° off-axis sample confirmed this trend, see Figure 2 b/, with magnitude of the transverse tensile component of the strain tensor not exceeding 5% of the shear component. The transverse stress, albeit very minor, is accounted for in the data reduction method.

2.3 *Sample preparation and test setup*

Two different toughed thermoset prepreg systems, representative of those used for primary structures in the aeronautical industry, are considered here: IM7/8552 and IMA/M21 from Hexcel®.

Some physical characteristics of the materials (i.e. fibre volume fraction, resin content and cured ply thickness) are provided in Table 1. The two systems are interesting to compare as they are examples of two different toughening strategies. IM7/8552 is toughened through the introduction of a sub-micron phase separating thermoplastic material that is dissolved in the uncured thermosetting epoxy resin whilst IMA/M21 is characteristic of the class of interlayer toughened thermosetting epoxy system that feature thermoplastic particles on the order of tens of microns, which are responsible for the creation of a resin-rich region between the plies [15]. The rheology of the two resin systems is well studied [34,35,37–39], and literature data [40] were used to make sure that all the tests were conducted within the range of temperatures and time scale where no substantial change of the degree-of-cure occurs. It has been shown by Hubert et al. [40] that in an isothermal test, considerable change in viscosity of 8552 resin only occurs at 110ºC after much longer time scales (above 60 min) than those the specimens were kept in the thermo-chamber in this study (i.e. less than 15 mins for the longest test performed).

Uncured prepregs are very compliant and can easily undergo wrinkling when excessively deformed in-plane. The specimens were made from more than one layer to avoid the potential local weakness at tow interfaces that may lead to very low strain for a single layer [30]. This also helped delay the onset of out-of-plane buckling for as long as possible, as when the tape buckles in-plane, shear is no longer the dominant mechanism and the collected data become irrelevant. All the specimens were laid-up by hand by stacking a defined number of layers (with the fibres at 10^{o} with respect to the main sample axis). A one hour long debulk cycle under vacuum was applied to consolidate the specimens into a single thick layer. Thickness were then measured at three different positions of the sample using a Vernier Caliper and the average value was calculated and recorded.

As illustrated in Fig. 3, the experimental setup includes a DIC system, a universal testing machine, and temperature chamber. At room temperature a Hounsfield single column displacement-control test machine with 500 N load cell was used (Fig. 3 a/). It allows to apply test rates varying from 0 to 500 mm/min with a minimum increment of 0.1 mm/min and a maximum displacement of 1 m. The samples were installed in the testing machine with roller grips with the top one having some rotational degree of freedom to help minimizing out-of-plane deformation during the test. For the test at elevated temperature (see section 4), a 1 kN load cell Shimadzu universal test machine with a thermal chamber, where the temperature can vary from 25^{o} C to 100^{o} C, was used (Fig. 3 b/). The minimum value that can be measured is around 2 N, with error within ±0.5%. A 5 Mega Pixel LaVision DIC system was used to monitor the deformation and obtain the evolution of the distribution of the different strain components on the specimen surface during the test. Normal LED lights were used to illuminate the specimen surface at room temperature. At elevated temperatures, the DIC cameras were mounted vertically due to the size of the thermal chamber's window, and LED strip lights were used inside the thermal chamber to prevent

light reflecting off its glass window. Since the temperature set in the chamber may differ from the actual temperature on the sample, a thermocouple (attached directly to the region of the sample where the strain localises) was used to measure the surface temperature of the prepreg and make sure that the applied temperature was known in the area where strains and stresses were measured. Both, the thermocouple and the chamber monitor showed that the temperature stabilizes between 5 and 7 mins. Tests were conducted after the temperature stabilized. Depending on the test cases, the testing time was between 10 s and 5 mins. An analogue-Digital Converter (ADC) was set to synchronise the load from both test machines.

In order to create a pattern on the specimens' surfaces, that is trackable by the DIC system, the samples were speckled using acrylic paint creating a fine black-on-white pattern that was shown, in trial tests, to give less light reflection and better image capture compared with white-on-black pattern. The entire loading process from the start to the complete loss of the samples integrity was captured by the DIC system and then post-processed with the LaVision Davis software. It is also worth noting that prior to the designed tests, the influence of acrylic paint was evaluated through comparing the load-displacement curves of samples with and without paint. These tests show minimal effect of the paint on the load applied. To reduce the initial torsion of the rigs, a small pre-load (around 1 N) was applied on the samples.

2.4 Data reduction procedure

As discussed before, the components of the strain tensor (including the shear and small transverse tensile constituents) within the shear band can be directly and separately extracted from the DIC. The strain calculation in the Davis software is based on Eq. (5), where *du* and *dv* are the differences between the x-components and y-components of every two adjacent vectors. The parameters *dx* and *dy* correspond to the distance between the centres of each adjacent interrogation cell.

$$\varepsilon_x = \frac{du}{dx} \quad \varepsilon_y = \frac{dv}{dy} \quad \gamma_{xy} = \frac{dv}{dx} + \frac{du}{dy} \tag{5}$$

The results are expressed with respect to the global (i.e. the lab) coordinate system. A coordinate transformation is therefore needed to obtain the local strain (i.e. with the x axis aligned with the fibre direction). The transformation equation is shown as Eq. (6), where ε_x /ε_y/ε_{xy} are the strain in global x/y directions, obtained directly from DIC while ε'_{xy} is the local shear strain with the initial value equal to 0 when tests begin . Θ is the transformation angle, here $\Theta_{int} = 80°$. The fibre rotation, mainly caused by the local shear strain within the band, was also considered to make the calculation more accurate, as shown in Eq. (7).

$$\varepsilon'_{xy_i} = 2 \cdot (\varepsilon_{y_i} - \varepsilon_{x_i}) \sin\Theta_i \cos\Theta_i + \varepsilon_{xy_i} (\cos^2\Theta_i - \sin^2\Theta_i) \tag{6}$$

$$\Theta_{i+1} = \Theta_i + 2\varepsilon'_{xy_i} \tag{7}$$

The shear stress can be obtained by resolving the local stress state of the shear band using the applied load, as Eq. (3). These equations are effective when the side length of the highly sheared region remains constant. As the test proceeds and the specimen extends, geometric nonlinearity occurs because of the rotation of fibres due to local shear strain, which must be taken into account. To correct for the fibre rotation occurring during the test, a Cauchy stress transformation tensor was introduced to the calculation as Eq. (8), where τ_{xy} is localised shear stress in the 'shear band' calculated by Eq. (3), θ_{int} is the initial off-axis angle of the specimen (i.e. 10°), $\Delta\theta$ is the increment of angle evolution during the test which is continuously recorded by the DIC camera and extracted directly from DIC results. In reference to the definition of shear strain in Eq. (5), $\Delta\theta$ is equal to $2\varepsilon'_{xy_i}$, obtained in Eq. (6).

$$\tau'_{xy} = \tau_{xy} \cdot \frac{\sin\big(2(\theta_{int} + \Delta\theta)\big)}{\sin(2\theta_{int})} \tag{8}$$

These transformations were necessary as prepreg tapes are very compliant and undergo large deformation. The relatively simple geometry and loading of the test that allows to derive Eq. (3) and the ability to collect all the in-plane components of the strain tensor, thus, makes it relatively simple to separate the in-plane shear and transverse tensile behaviours of the material.

3. Exploratory room temperature tests

3.1 Test configurations

A challenge of the test programme is to separate the apparent and actual material responses. This firstly requires establishing whether the material and sample behaviour are size dependent or not. Hence, the material needs to be tested for various tape width and sample thickness. In addition, because of viscous nature of the resin, the material needs to be tested at various rates. A first series of tests were performed at room temperature. Different thicknesses (3, 4, 5 layers), "tow" widths (6 mm, 8 mm) and test rates (0.001/s, 0.01/s, 0.05/s) and were studied. Five specimens were manufactured and tested in each case. All combinations, of thickness, width and test rate where studied, leading to 75 tests in total for each of the 2 prepreg types considered. The dimensions of the specimens were set using Eq. (4) and considering the width of fixture on the test machine, the off-axis angle and desired width of the localisation area. The corresponding sample dimensions (except the grip area) were respectively 261.4 mm × 40 mm and 273 mm × 40 mm for a tow width of 6 mm and 8 mm respectively. The test set-up is shown in Fig. 3 a/.

3.2 Representative sample behaviour and data extraction procedure

During the test process, samples undergo wrinkling when excessively deformed in-plane. Hence, the data obtained during the test process are not fully usable. In this section, a representative sample is used to illustrate the data extraction procedure followed to determine a material law (i.e. shear stress vs shear strain curve) from the experiments performed.

For every test case, the load applied and displacement of the grips with respect to time were recorded by the test machine along with the independent strain assessment by DIC. All of the collected curves displayed a similar behaviour, A representative shear load-displacement curve of the baseline specimens made by stacking up 3 plies of IM7/8552 and with 8 mm-wide shear region is shown in Figure 4. At the start of the deformation, the load-displacement curves are linear (after an initial settling in stage where the sample becomes fully engaged with the applied load). As load continues to increase, there is a turning point on the curve, after which the load increases more slowly for the same displacement rate.

The in-plane components of the strain tensor (ε_x /ε_y/ε_{xy}) and the out of plane deformation were captured by DIC. The subset and step size used were 1.5 mm and 0.75 mm, respectively. Figure 5 shows the evolution, at fixed time intervals, of ε_{xy} (Fig. 5 a/) and the out-of-plane deformation (Fig. 5 b/) for one representative specimen. The strain maps show that, as intended, as the load increases, a localised shear band is formed. The shear band, defined as an area where the component ε_{xy} is much higher than in the rest of the specimen, gradually develops and becomes more and more pronounced as the samples get closer to disintegration. Within this band, the deformation is relatively uniform. The shear strain for a particular sample at a given time interval is calculated by performing the transformation described by Eq. (5) for each point in the band and then averaging out the data. Fig. 5 /b shows the evolution of the out of plane deformation during the test. Due to the high compliance of the prepreg, it is nearly impossible to place the samples in the test machine so that they are perfectly planar. A slight edge rotation of the specimen (that the DIC system can correct for) is, therefore, observed at the start of the test. As the applied load increases, out-of-plane wrinkles progressively appear as shown on Fig. 5 b/. The data reduction procedure (see section 2.4) assumes that the deformation only happens in-plane. It therefore becomes inaccurate as the experimental conditions diverge from this. This forms the basis for disregarding any data collected past the onset of out-of-plane wrinkling.

As illustrated in Fig. 6, where the distribution of the out-of-plane deformation along the centre line of the specimen is plotted for different load levels, the wrinkles' amplitudes increase drastically when the load exceeds 150 N (for the considered specimen). This correlates well with the point at which the load-displacement curve in Fig. 4 diverges from linearity (i.e. the 'turning point'). This inflection is thus inferred to relate to out-of-plane wrinkling. The judgement on when data needs to be disregarded is thus based on the inspection of both the load-displacement curve and the out-of-plane deformation DIC data.

The strain extraction from DIC and the stress calculation using the applied load, together with the out-of-plane judgement, pave the way for obtaining the shear stress-strain behaviour. The DIC system was synchronised with the test machine so that the strain tensor components and applied load acquisitions could be collected simultaneously, easing the construction of the stress-strain curves. A representative

example of a shear stress versus shear strain curve thus obtained is displayed in Fig. 7. The stress at the buckling load (obtained from previous step) was calculated and marked on the curve as the onset of wrinkling. The section after the red line should therefore be disregarded. Thus, the extraction of usable data for in-plane shear behaviour is completed. The usable result, which is enlarged in the right-bottom corner of the graph, indicates the shear stress versus shear strain exhibits a nonlinear relationship.

3.3 Effect of the specimen geometry

3.3.1 Effects of the sample thickness on the measured behaviour

As stated before, the test samples were made by laying up several layers of prepreg with the same fibre orientation. A common phenomenon in heterogeneous materials is the existence of size-effects[15]. The influence of the specimen thickness on the measured in-plane shear behaviour was therefore investigated with this consideration in mind. Samples made from IM7/8552 and IMA/M21 were manufactured using 3, 4 and 5 layers respectively and tested at the 3 test rates mentioned in section 3.1. A variant of this with a 6 mm wide shear band was also trialled. As all these variations showed the same trend, only the results corresponding to the samples with an 8 mm wide deformation localisation area are presented here.

In the cases of both IM7/8552 and IMA/M21 samples, the buckling loads were shown to increase with the layer thicknesses, as shown in Fig. 8. As expected, the thicker specimens exhibit higher critical buckling loads. The main reason that the IMA/M21 samples reached higher loads than the IM7/8552 ones is likely to be because that it has thicker plies (0.21 mm vs 0.165 mm).

The shear stress-strain curves obtained for these cases are shown in Fig. 9, where the solid line represents the average for the 5 repeats, while the standard deviation, calculated as Eq. (7), was depicted by the coloured band, where x_i is the shear stress obtained at given shear strain and $\bar{x}$ is the mean value. N is the number of samples tested. All the specimens exhibited similar trends and significant overlaps can be observed. This demonstrates that the variation of the extracted material behaviour with the specimen's thicknesses is small compared to the natural scatter in material response.

$$stdev = \sqrt{\frac{1}{N-1}\sum_{i=1}^{N}(x_i - \bar{x})^2} \tag{9}$$

3.3.2 Influence of the width of localisation area

One of the parameters that varies the most from one AFP machine to another is the width of the tape. It is a key parameter in the formation of defects as narrower tape widths allow smaller critical radii as there is less distance from the neutral axis to the edge of the tape and the in-plane compressive loads (at the inner edge) and tensile loads (at the outer edge) due to in-plane bending are decreased. The deposition of narrower bands has, thus, been one of the main improvements of the AFP technology in

comparison to the Automated Tape Laying (ATL) method which mainly allows to deposit material on flat surfaces following straight deposition paths. A trade-off between the geometrical complexity of the parts a machine can handle and the maximum deposition rate, however, needs to be considered as it takes longer to cover a surface with narrower strips of materials.

To investigate if/how the tape width influences the apparent in-plane shear properties of the prepreg, samples were designed so that the widths of the localisation area were 6 mm and 8 mm respectively. In a similar manner to the study on the effects of the tape thicknesses, the average value and error range for the 2 test widths were calculated and gathered together. Fig. 10, where shear stress versus strain curves (and the band in which they vary from sample to sample) for each case are plotted, shows that there is no apparent size-effects to be considered in relation with the width of the tape for material IMA/M21 (Fig. 10 b/). In the case of IM7/8552 (Fig. 10 a/), the curves corresponding to the tested width do not formally overlay at very low strain, however, the difference was deemed to be small enough to not investigate this further. The same trend was observed whatever the specimen thickness or test rate. Therefore, only the tests corresponding to the 3 layers-thick sample tested at 0.01/s are presented here.

3.3.3 Influence of the test rates

The deformation rate, dominated by behaviour of the viscous resin, is another key parameter. The AFP deposition process is slowed down for features having geometrical complexity, to reduce the severity of steering defects, because the material becomes more compliant at lower rates. However, to the best of our knowledge, most of the experimental data available in the open literature were obtained from tests conducted at rates several orders of magnitude lower than those applied in real manufacturing processes. It is shown in section 2.1 that shear strain rates of 0.2-0.5 s^{-1} can be expected in the steering of a prepreg tape by an AFP robot. In the present section, it is demonstrated that although the equipment does not reach deformation rates as high this, it still makes it possible to investigate a much wider rate spectrum than any other set-up used for thermoset prepregs in past literature [10]. Testing rates of 0.001/s, 0.01/s, 0.05/s were selected.

Since the variation of shear rate is achieved by changing the crosshead speed rather than being controlled directly, a comparison between the set test rate and real shear rate is shown in Fig. 11 a/, where the mid-test rate was chosen for illustration. It can be seen the shear rate is mostly constant except when the test is initialised, for strain less than 1%. Fig. 11 b/ shows an example of the effect of the testing rate of IM7/8552 samples made from 5 layers and where the width of the deformation localisation area was set to 8 mm. At a given strain, the recorded stresses vary almost linearly with the applied rate, as shown in Fig. 11 c/.

4. Shear behaviour of IM7/8552 and IMA/M21 prepreg under processing conditions

4.1 Test configurations

The preliminary tests described in section 3 demonstrate the feasibility of the proposed test methodology for 2 types of prepreg with different micro-structural morphology. They also showed that, under shear loading, prepregs do not exhibit size effects and that there is, therefore, no need to study the influence of the samples' sizes on the measured behaviour. In this section, a more quantitative study with better control of the environmental constraints is performed.

The test set-up illustrated in Fig. 3 /b and discussed in section 2.3 is used. The dimensions of the samples were amended slightly to 23 mm × 207 mm to adapt to the different size of grips between the Hounsfield test machine used at room temperature and the Shimadzu machine used here. As the width and thickness of the samples were shown to have little influence on their in-plane shear behaviour, the width of the localisation band was fixed at 6.35 mm (i.e. 1/4 inch, which is a widespread width for AFP tape) and the thickness was set to 5 layers to allow for higher buckling loads (thus widening the number of points that can be used in the derivation of the stress-strain curves, as discussed in section 3.2). Again, both IM7/8552 and IMA/M21 were studied.

To decrease the size of the test matrix, a quick screening of the influence of temperature was performed. Tests were conducted at temperature ranging from 25°C to 85°C with a 10°C increment. Only one sample was used in each case. The "buckling load" (i.e. the 'turning point' on the load vs displacement curve) was used as indication of the evolution of the material properties. A representative curve of the evolution this buckling load with the testing temperature for IM7/8552 is shown in Fig. 12. A significant decrease of the buckling load is observed between 25°C and 60°C and the decline of the tape resistance to shearing slows down greatly after that. This is in good agreement with the known evolution of the resin viscosity with temperature [34,35] and other studies on consolidation [14] that showed a plateauing behaviour above 70°C. Based on these observations, it was decided to perform a detailed study at 25°C, 50°C and 75°C (which should be sufficient to capture the overall shape of the curve in Fig. 12). Test rates of 0.001 s^{-1}, 0.01 s^{-1} and 0.1 s^{-1} were examined at each of these temperatures. Five test repeats were conducted for each temperature and test rate. The corresponding test matrix is can be found in Table 2.

4.2 Effect of the applied loading rate

Fig. 13 shows the shear stress-strain curves at different temperatures (25ºC/50ºC/75ºC) under each test rate (0.001 s^{-1}/0.01 s^{-1}/0.1 s^{-1}) for IM7/8552 and IMA/M21 prepreg. Good consistency between test repeats is obtained. The solid lines represent the average shear stress-strain curves, with the abrupt changes in the trend corresponding to the exclusion of one or more samples due to buckling. The coloured bands represent the variation in the maximum and minimum values of shear stress obtained for the five repeats at different strain rates. A nonlinear relationship between the shear stress and shear strain is

observed, with the largest linear slope at small shear strain. This is in accordance with the viscoelastic characteristics of the uncured prepreg. The linear response dominates at the very start of the material's behaviour. It is followed by a delayed viscous response a short time later. This also contributes to the phenomenon that the higher the strain rate the larger the initial linear portion at all temperatures.

For all the temperatures, the higher test rates lead to higher shear stress at a given strain. This seem to be related to the microstructure of the prepreg. Deignan et al. [41], working on fibre reinforced thermoplastic melts, have suggested that the resistive forces between two fibres increases with shear rate. At low strain rates, friction between lubricated fibres provides most of the resistive force, with little resistance from the shearing of the resin. Conversely, for high strain rates, increased pressure in the resin can result in the fibres being pushed apart, while the resistance from the shearing of the resin becomes dominant. This indicates that the interaction between fibres embedded in uncured prepreg seems to follow the trend in the mixed lubrication stage in a Stribeck curve. Even though the resin viscosity at high strain rate is slightly lower due to some level of shear thinning [38], more load is transferred from the viscous resin to the stiff fibres following a large increase in strain rate. This would, in turn, lead to higher shear stresses as observed in the experimental results reported here. This micro-scale fibre to fibre interaction is not accounted for in traditional microscale models of composites manufacturing that assume the fibres be rigid rods that do not interact with each other. An apparent exception to this general behaviour is observed at highest test rates (i.e. at shear strain < 1.5% and 0.1/s test rates) where the initial elastic shear modulus seems to decrease with the applied rate. It may be due to the small amount of slippage of the samples in the grips.

4.3 Effect of processing temperature

To ease interpretation on the effect of temperature, the same set of data was replotted in Fig. 14, where shear stress-strain curves for different temperatures, but at the same test rate, are plotted on a same graph. The results indicate that compared to test rates, the temperature has a more pronounced influence on the material behaviour. The variation of the recorded stresses between 25ºC and 50ºC is much larger than between 50ºC and 75ºC. This is in accordance with the temperature screening result mentioned in section 4.1 and the known evolution of the resin's viscosity with temperature for the 2 systems considered [39,40].

The large variation between individual tests in the case of 25^{o} C at 0.001/s for IMA/M21, as depicted by relatively wider band in Fig. 14 a/, reveals one potential source of experimental inaccuracy. In this case, the five repeats were tested over two days (first three on one day, and the other two the next day). Since there is no control of the ambient humidity, the humidity difference between the two days may lead to a difference. This is supported by the fact that test repeats conducted on the same day had much a smaller variation. Work by Netzel et al. [42] also suggests that the humidity has an obvious influence of

the compaction behaviour for stacked cross-plied prepreg tapes in Ramp-Dwell compaction test. Ideally, all the testing should be conducted in a controlled humidity environment.

4.4 Comparison of the behaviour of IM7/8552 and IMA/M21

Figs 13 and 14 show a side-by-side comparison between the in-plane shear results for IM7/8552 (left) and IMA/M21 (right) UD prepreg with consistent axes. Overall, both materials have shown that varying the process temperature and applied load rate has a significant influence on their in-plane shear behaviour. The shear stresses recorded were relatively similar in magnitude, but the rate of increase in shear stresses with shear strains was higher in IM7/8552 prepreg when compared to the IMA/M21. Moreover, the onset of out-of-plane wrinkling occurred at higher shear strains and buckling loads for IMA/M21 than for IM7/8552 system. This is not unexpected due to the difference in thickness of the individual plies between the 2 types of prepregs (averaging 0.21 mm for IMA/M21 vs 0.165 mm for IM7/8552 in the uncured state) that will result in higher out-of-plane bending stiffness for IMA/M21.

As already alluded to, a major difference between the two prepreg system is the type of toughening strategy used, that affects their respective meso-scale morphology [15,26]. The IMA/M21 material includes thermoplastic particles at the ply interfaces. The micrographs in figure 15 illustrate this difference clearly, with the IM7/8552 system have a much more homogenous microstructure, compared to the layered microstructure of IMA/M21. The distribution of the shear strain (ε_{xy}) in the global coordinate system (obtained through DIC) shown in Fig. 15 indicates that compared to the relatively uniform shear band in IM7/8552, several parallel bands appear in the shear band of IMA/M21. This could be due to the layers of thermoplastic-interleaf at the interface between the plies, which leads to a more heterogenous microstructure and local variations of the ply thickness. This subsequently results in less homogeneous stresses and strains fields in the localisation area. These observations are consistent with Larberg et al. [26] and Potter [20], where the presence of resin-rich areas between the tows was assumed to cause local variation and higher shear stresses to form. On the other hand, for the IM7/8552 system (also shown in Fig. 15) fibres are more homogenously distributed and the original ply structure almost disappears. This allows for a single diagonal band of high ε_{xy} to form in the middle of the sample as designed.

5. Conclusions

In this paper, the in-plane shear characterisation of uncured thermoset prepreg was studied using a 10° off-axis tensile test. Two commonly used aerospace grade thermosetting epoxy prepreg systems, IM7/8552 and IMA/M21, were selected for the study. Different test rates and temperatures, chosen to broadly cover the same range as that of a real manufacturing process such as AFP and thermoforming. The temperature range (25-85 ºC) and high deformation rates (0.01/s - 0.1/s) roughly cover the spectrum seen in the AFP deposition process as documented in [1] and in section 2.1 of the present contribution. If

a similar programme with application to other manufacturing technique such as thermoforming was required, then higher deformation rates could be reached if using a load cell of higher capacity. The test has several advantages:

- loads are applied using a widely available universal testing machine making it easy to conduct;
- elevated temperature testing can be done using a thermal chamber;
- samples manufacturing only requires stacking a few sheets on top of each other and is relatively quick;
- the applied shear strains can be directly measured optically by DIC;
- the size of the zone in which strain localises can be controlled by varying the sample dimensions offering an easy route to study potential size-effects [15].

In contrast to the behaviour of prepreg in consolidation [14], no distinct size effect was observed. However, as would be expected, due to the presence of uncured resin in the systems considered, strong dependencies on both temperature and applied shear rate were observed. The results indicate that the method provides a good way to characterise the in-plane shear behavior of thermoset prepreg under processing conditions as it is relatively simple to implement, does not rely on complex data reduction with assumed boundary conditions which may or may not be satisfied in the real tests and allows to explore a range of testing parameters that are consistent with real manufacturing conditions. The collected set of data provides a solid base against which robust models for composite manufacturing simulation can be built.

However, more work in this area is necessary considering the complexity of uncured prepreg's behaviour. As shown in Fig. 16, the test results indicate the linear slope between the stress and strain of the material's 'apparent Young's Modulus', varies with the applied rate (i.e. the initial behaviour is not purely elastic). Also, the fibre friction and fibre-melt interaction are highlighted in the section 4.2 for interpretation which are consistent with the findings of Deignan et al. [41]. This suggests that the commonly used phenomenological approaches such as standard linear visco-elastic models and micro-mechanics based models such as those from Christensen [28] or Pipes et al. [29] may fail to capture the observed behaviour. More advanced models therefore will need to be developed in future to describe the material behaviour.

Acknowledgement

This work was funded by the Engineering and Physical Sciences Research Council (EPSRC) through the Centre for Doctoral Training in Advanced Composites for Innovation and Science (grant no. EP/L016028/1) and the EPSRC platform grant "Simulation of new manufacturing Processes for

Composite Structures (SIMPROCS)" (grant no. EP/P027350/1). The authors would also like to thank Dr Steven Rae in the lab support team and Dr Marco Longana for their help on DIC system usage.

References

[1] Lukaszewicz DHJA, Ward C, Potter KD. The engineering aspects of automated prepreg layup: History, present and future. Compos Part B Eng 2012;43:997–1009.

[2] Poursatip A. Transitioning Composites Manufacturing Simulation into Industrial Practice: Challenges and Opportunities. ICMAC 2015-International Conf. Manuf. Adv. Compos. Bristol, United Kingdom, 2015.

[3] Boisse P, Hamila N, Madeo A. The difficulties in modeling the mechanical behavior of textile composite reinforcements with standard continuum mechanics of Cauchy. Some possible remedies. Int J Solids Struct 2018;154:55–65.

[4] Harrison P, Alvarez MF, Anderson D. Towards comprehensive characterisation and modelling of the forming and wrinkling mechanics of engineering fabrics. Int J Solids Struct 2018;154:2–18.

[5] Haanappel SP, Ten Thije RHW, Sachs U, Rietman B, Akkerman R. Formability analyses of uni-directional and textile reinforced thermoplastics. Compos Part A Appl Sci Manuf 2014;56:80–92.

[6] Guzman-Maldonado E, Hamila N, Naouar N, Moulin G, Boisse P. Simulation of thermoplastic prepreg thermoforming based on a visco-hyperelastic model and a thermal homogenization. Mater Des 2016;93:431–42.

[7] Beakou A, Cano M, Le Cam JB, Verney V. Modelling slit tape buckling during automated prepreg manufacturing: A local approach. Compos Struct 2011;93:2628–35.

[8] Matveev MY, Schubel PJ, Long AC, Jones IA. Understanding the buckling behaviour of steered tows in Automated Dry Fibre Placement (ADFP). Compos Part A Appl Sci Manuf 2016;90:451–6.

[9] Belhaj M, Hojjati M. Wrinkle formation during steering in automated fiber placement: Modeling and experimental verification. J Reinf Plast Compos 2018;37:396–409.

[10] Hormann P. Thermoset automated fibre placement on steering effects and their prediction. Technical University of Munich, 2015.

[11] Bakhshi N, Hojjati M. An experimental and simulative study on the defects appeared during tow steering in automated fiber placement. Compos Part A Appl Sci Manuf 2018;113:122–31.

[12] Dörr D, Henning F, Kärger L. Nonlinear hyperviscoelastic modelling of intra-ply deformation behaviour in finite element forming simulation of continuously fibre-reinforced thermoplastics. Compos Part A Appl Sci Manuf 2018;109:585–96.

[13] Wang P, Hamila N, Boisse P. Thermoforming simulation of multilayer composites with

continuous fibres and thermoplastic matrix. Compos Part B 2013;52:127–36.

[14] Belnoue JPH, Nixon-Pearson OJ, Thompson AJ, Ivanov DS, Potter KD, Hallett SR. Consolidation-driven defect generation in thick composite parts. J Manuf Sci Eng Trans ASME 2018;140.

[15] Nixon-Pearson OJ, Belnoue J-HPH, Ivanov DS, Potter KD, Hallett SR. An experimental investigation of the consolidation behaviour of uncured prepregs under processing conditions. J Compos Mater 2017;51:1911–24.

[16] Amini Niaki S, Forghani A, Vaziri R, Poursartip A. An Orthotropic Integrated Flow-Stress Model for Process Simulation of Composite Materials—Part II: Three-Phase Systems. J Manuf Sci Eng 2019;141:031011.

[17] McGuinness GB, ÓBrádaigh CM. Characterisation of thermoplastic composite melts in rhombus-shear: the picture-frame experiment. Compos Part A Appl Sci Manuf 1998;29:115–32.

[18] Harrison P, Clifford MJ, Long AC. Shear characterisation of viscous woven textile composites: A comparison between picture frame and bias extension experiments. Compos Sci Technol 2004;64:1453–65.

[19] Boisse P, Hamila N, Guzman-Maldonado E, Madeo A, Hivet G, dell'Isola F. The bias-extension test for the analysis of in-plane shear properties of textile composite reinforcements and prepregs: a review. Int J Mater Form 2017;10:473–92.

[20] Potter K. Bias extension measurements on cross-plied unidirectional prepreg. Compos - Part A Appl Sci Manuf 2002;33:63–73.

[21] Harrison P, Abdiwi F, Guo Z, Potluri P, Yu WR. Characterising the shear-tension coupling and wrinkling behaviour of woven engineering fabrics. Compos Part A Appl Sci Manuf 2012;43:903–14.

[22] Scobbo JJ, Nakajima N. Modification of the mechanical energy resolver for high temperature and rigid material applications. Polym Test 1990;9:245–55.

[23] Stanley WF, Mallon PJ. Intraply shear characterisation of a fibre reinforced thermoplastic composite. Compos Part A Appl Sci Manuf 2006;37:939–48.

[24] Groves DJ. A characterization of shear flow in continuous fibre thermoplastic laminates. Composites 1989;20:28–32.

[25] Groves DJ, Bellamy AM, Stocks DM. Anisotropic rheology of continuous fibre thermoplastic composites. Composites 1992;23:75–80.

[26] Larberg YR, Åkermo M, Norrby M. On the in-plane deformability of cross-plied unidirectional prepreg. J Compos Mater 2012;46:929–39.

[27] Haanappel SP, Akkerman R. Shear characterisation of uni-directional fibre reinforced

thermoplastic melts by means of torsion. Compos Part A Appl Sci Manuf 2014;56:8–26.

[28] Christensen RM. Effective viscous flow properties for fiber suspensions under concentrated conditions. J Rheol 1993;37:103–21.

[29] Pipes RB, Hearle JWS, Beaussart AJ, Sastry AM, Okine RK. A Constitutive Relation for the Viscous Flow of an Oriented Fiber Assembly. J Compos Mater 1991;25:1204–17.

[30] Potter K. In-plane and out-of-plane deformation properties of unidirectional preimpregnated reinforcement. Compos Part A Appl Sci Manuf 2002;33:1469–77.

[31] Schirmaier FJ, Dörr D, Henning F, Kärger L. A macroscopic approach to simulate the forming behaviour of stitched unidirectional non-crimp fabrics (UD-NCF). Compos Part A Appl Sci Manuf 2017;102:322–35.

[32] G. K. Batchelor. The stress generated in a non-dilute suspension of elongated particles by pure straining motion. J Fluid Mech 1971.

[33] Pipes, R. B., Hearle, J. W. S., Beaussart, A. J., Sastry, A. M., & Okine RK. A Constitutive Relation for the Viscous Flow of an Oriented Fiber Assembly. J Compos Mater 1990;25.

[34] Hexcel Corporation. HexPly ® 8552 Epoxy matrix (180°C/356°F curing matrix). 2016.

[35] Hexcel. HexPly ® M21 - Product Data Sheet - EU Version. 2015.

[36] Stephenson MJ, Ryan ME. Experimental study of the thermoforming of a blend of styrene-butadiene copolymer with polystyrene. Polym Eng Sci 1997;37:450–9.

[37] Mesogitis T, Kratz J, Skordos AA. Heat transfer simulation of the cure of thermoplastic particle interleaf carbon fibre epoxy prepregs. J Compos Mater 2019;53:2053–64.

[38] Wang jinhuo. Predictive modelling and experimental measurement of composite forming behaviour. University of Nottingham, 2008.

[39] Ee D V, Poursartip A. HexPly 8552 material properties database for use with COMPRO CCA and RAVEN. Natl Inst Aviat Res Wichita, KS, Accessed Oct 2009;12:2016.

[40] Hubert P, Johnston A, Poursartip A, Nelson K. Cure Kinetics and Viscosity Models of Hexcel 8552 epoxy resin. Int SAMPE Symp Exhib 2001:2341–54.

[41] Deignan A, Figiel, McCarthy MA. Insights into complex rheological behaviour of carbon fibre/PEEK from a novel numerical methodology incorporating fibre friction and melt viscosity. Compos Struct 2018;189:614–26.

[42] Netzel C, Bickerton S, Battley M, Hubert P.
Private communication, University of Auckland, CACM (2019)

Figures

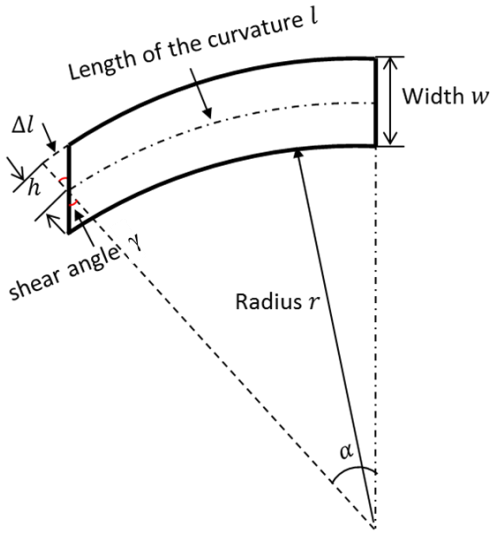

Fig. 1. Pure shear deformation of the prepreg in the steering process.

a/ b/

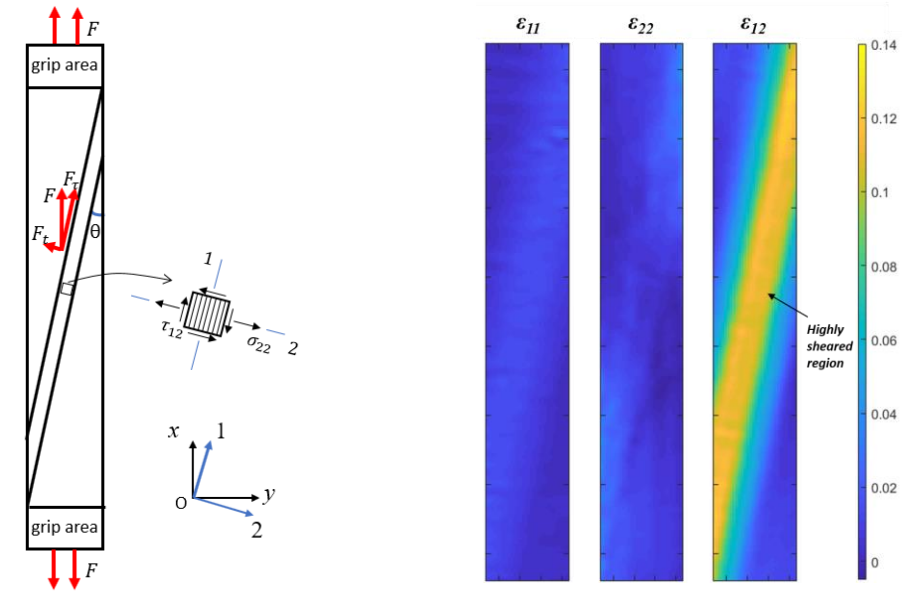

Fig. 2. Off-axis tensile test for uncured prepreg – a/ Schematic of test method and b/ Strain fields ($\varepsilon_{11}/\varepsilon_{22}/\varepsilon_{12}$) of a specimen in an actual test, obtained through DIC and rotated into the local coordinate system of the fibres

a/

b/

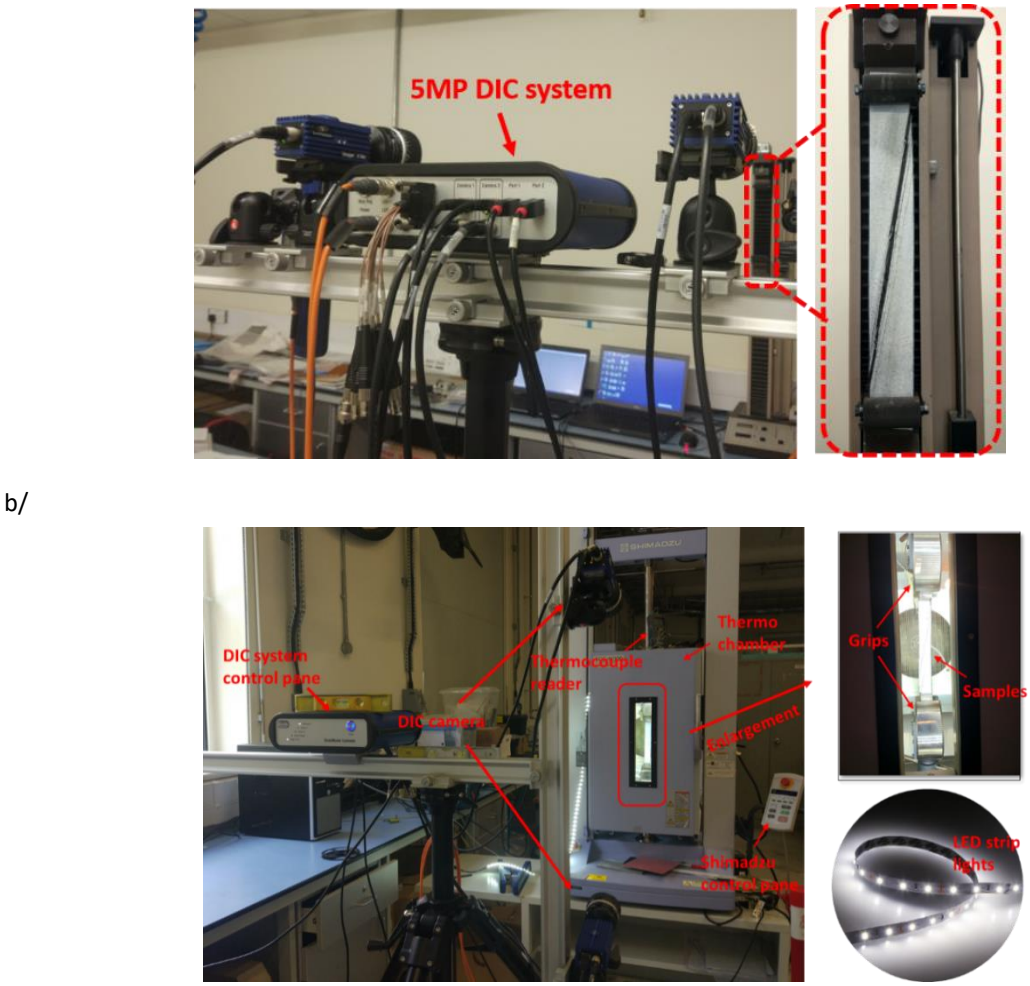

Fig. 3. Test set-ups for a/ Initial room temperature tests and b/ Elevated temperature tests.

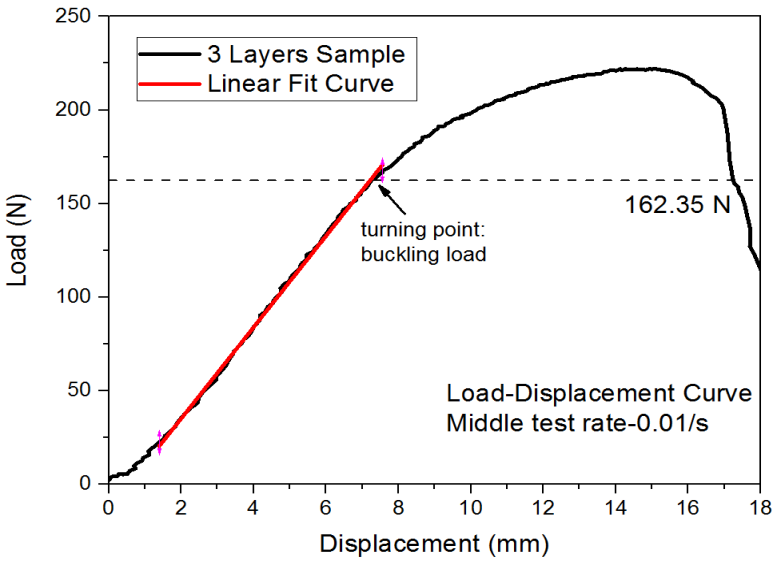

Fig. 4. Load-displacement curve of an IM7/8552 specimen of 3 plies thickness, 8 mm wide shear band tested at 0.01/s.

a/

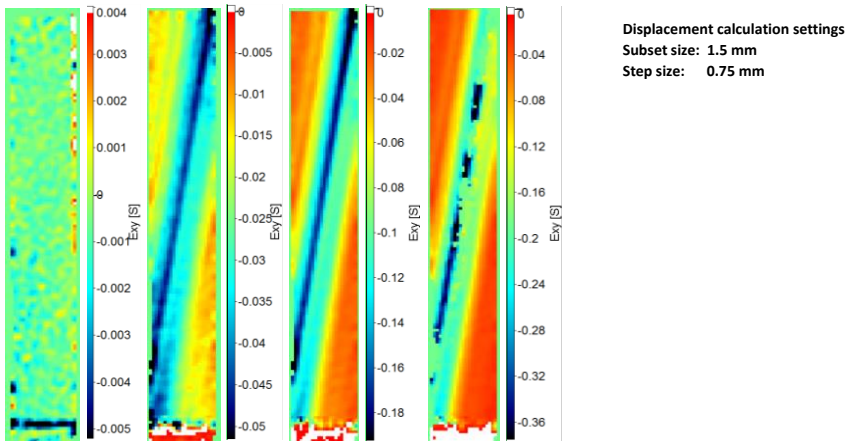

b/

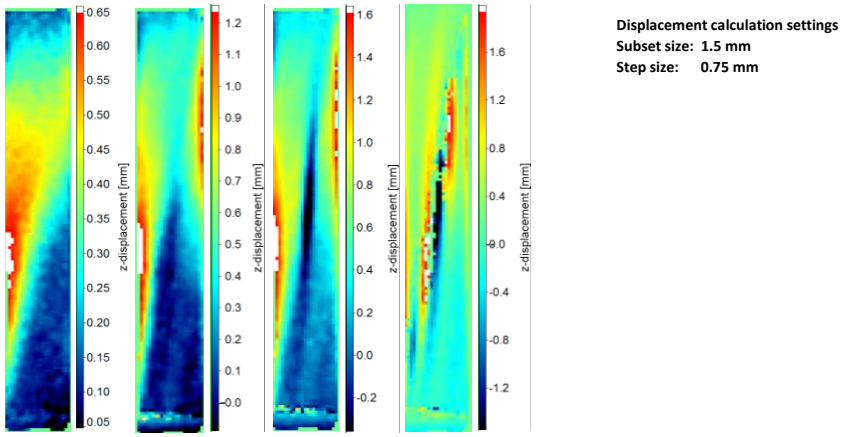

Fig. 5. DIC analysis results – a/ Shear strain field and b/ Out of plane deformation for an IM7/8552 specimen of 3 plies thickness, 8 mm wide shear band tested at 0.01/s.

a/ b/

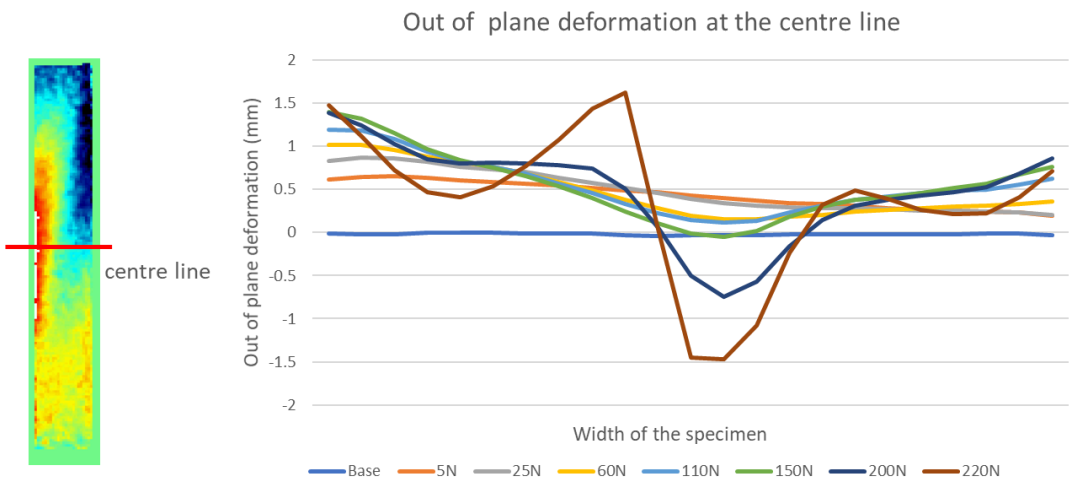

Fig. 6. Out of plane deformation at the centre line for a representative IM7/8552 specimen--a/ mark of the centre line and b/ the out of plane deformation along the line.

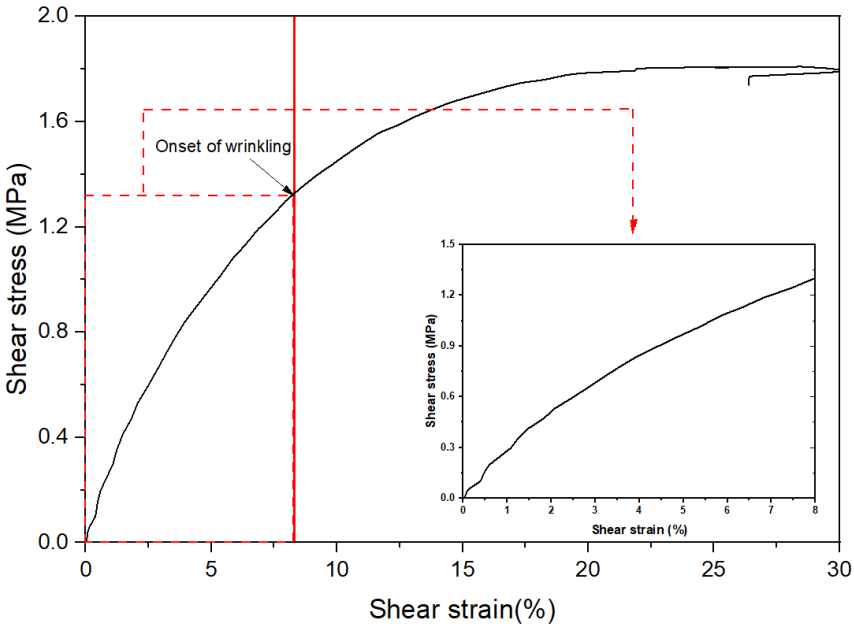

Fig. 7. A representative shear stress vs shear strain curve during the test.

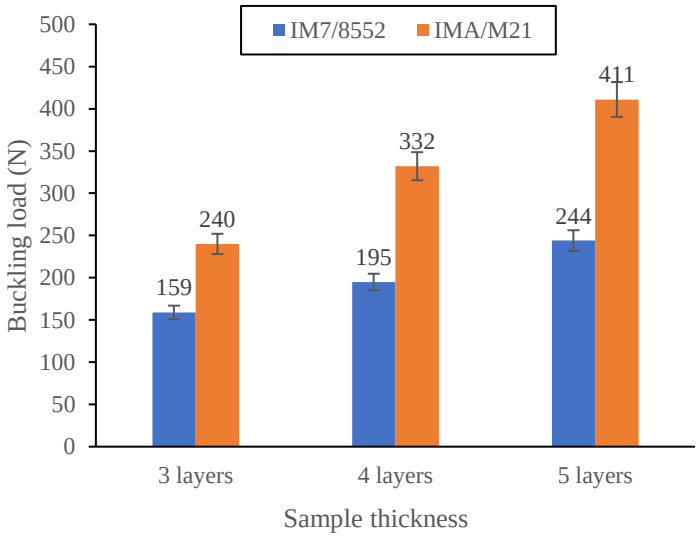

Fig. 8. Influence of the sample thickness on the measured buckling load.

a/ b/

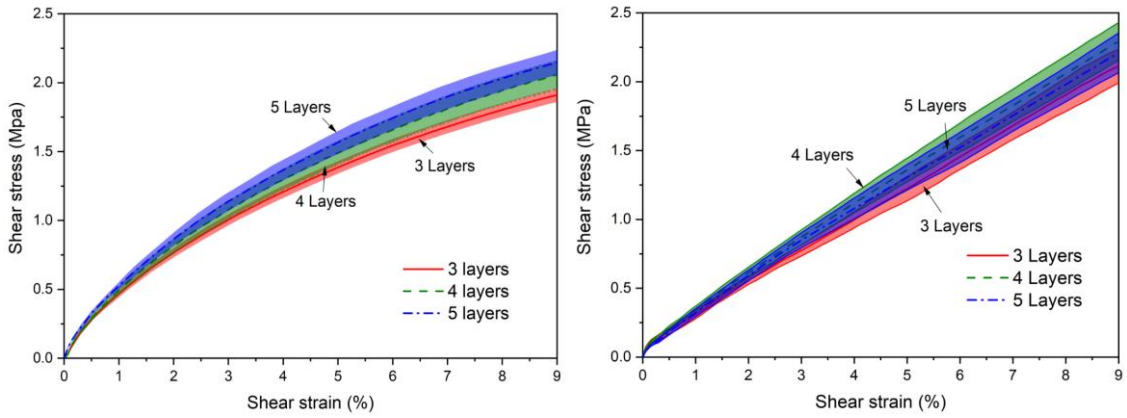

Fig. 9. Shear behaviour of specimen with different thicknesses for a/ IM7/8852 and b/ IMA/M21. The test rates were IM7/8852 (0.05/s), IMA/M21(0.01/s) and the width of the localisation area was 8 mm.

a/ b/

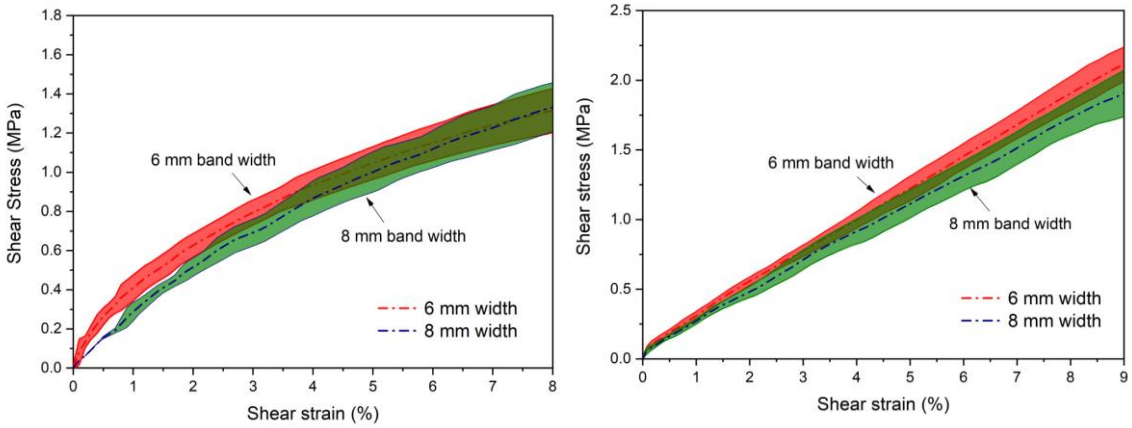

Fig. 10. Shear stress vs shear strain with different tape widths for a/ IM7/8852 and b/ IMA/M21. The test rate was 0.01/s and the samples were made of 3 layers each.

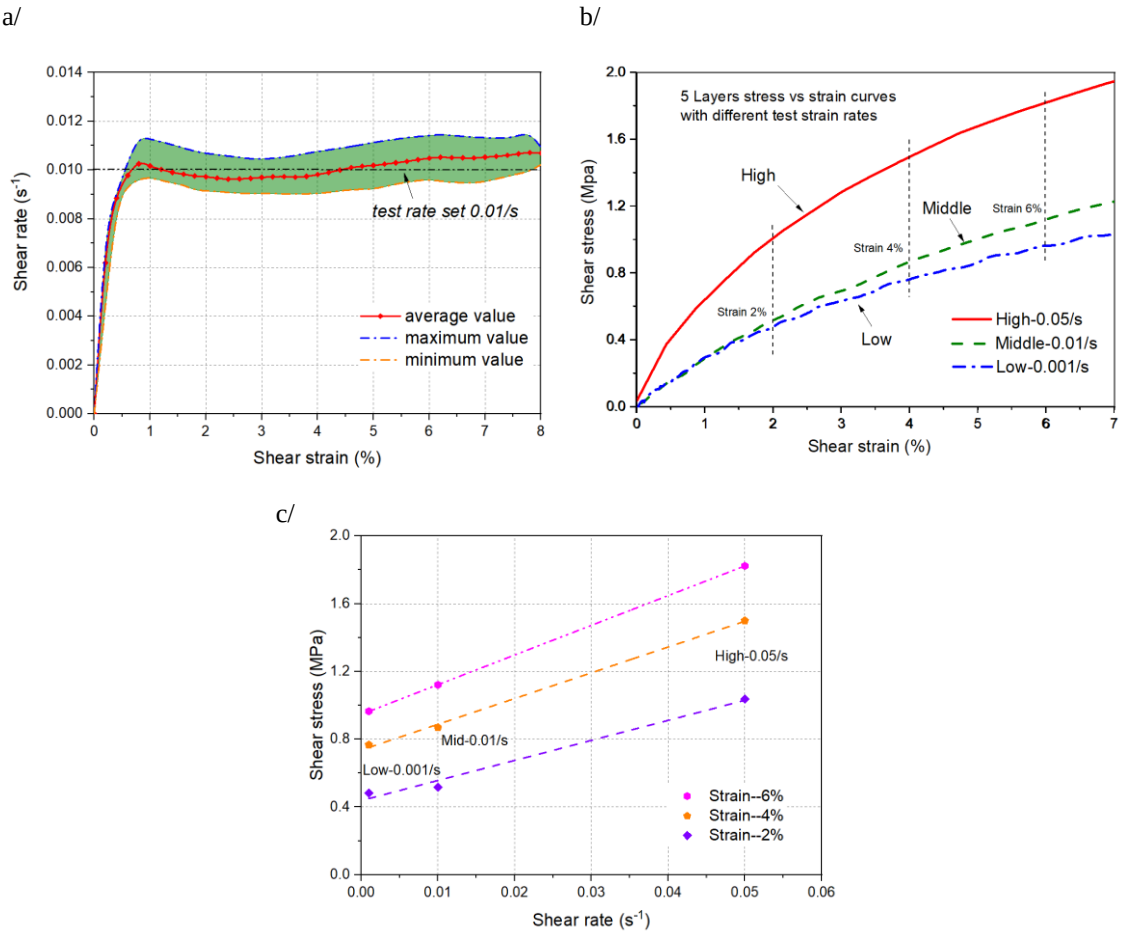

Fig. 11. Influence of the test rates – a/ Shear rate versus test rate, b/ Effect of test rates on IM7/8552 made of 5 layers and with an 8 mm-wide localisation area and c/ Shear stress versus shear rate at give strain extracted from Figure 11 b/.

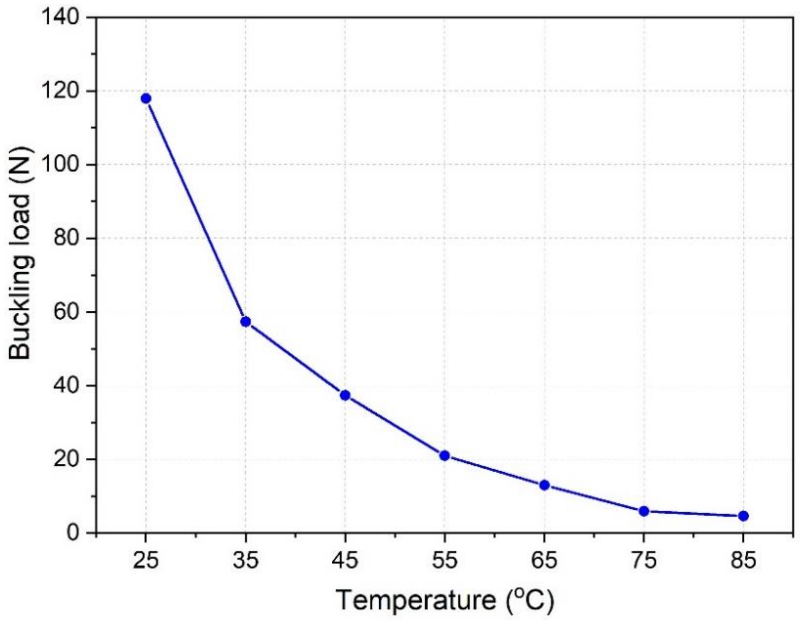

Fig. 12. The change in buckling load with temperature for IM7/8552.

a/

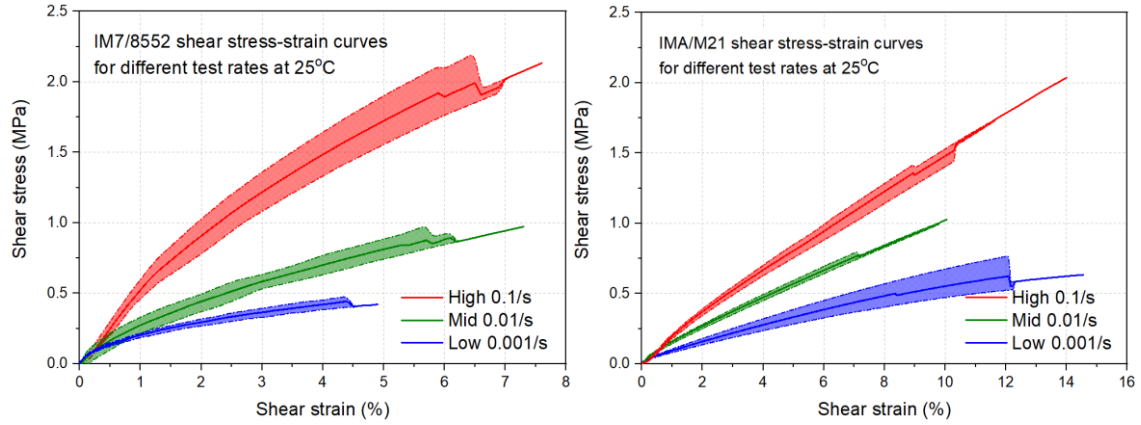

b/

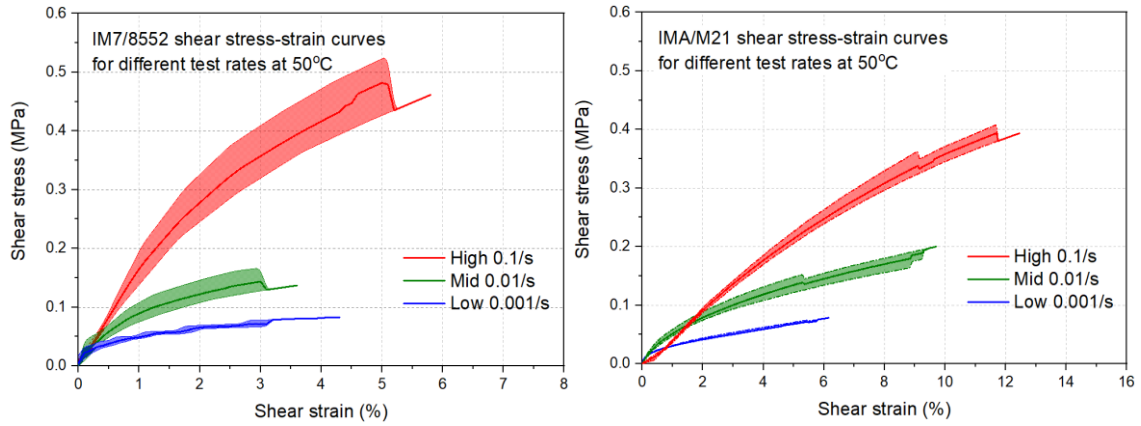

c/

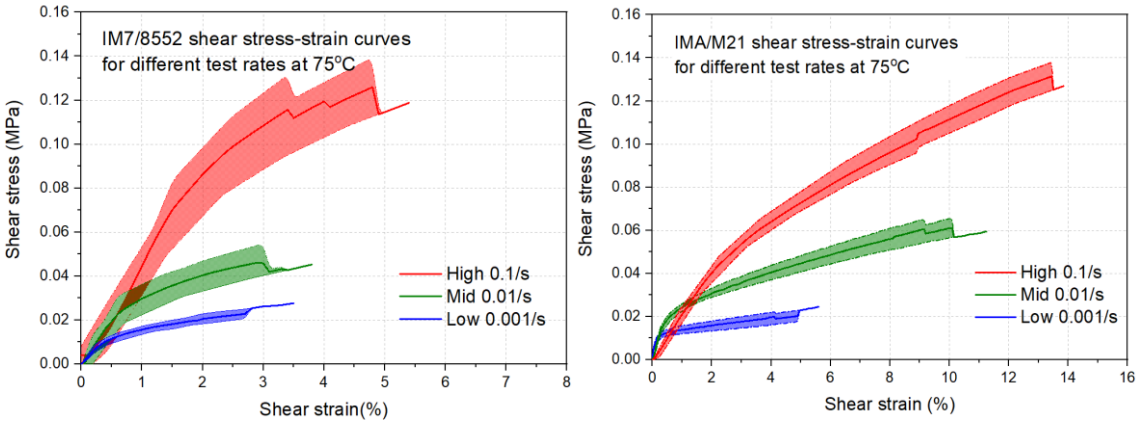

Fig. 13. Influence of test rate on the measured shear stress versus shear strain curves (left - IM7/8552 and right - IMA/M21) at a/ 25ºC, b/ 50ºC and c/ 75ºC.

a/

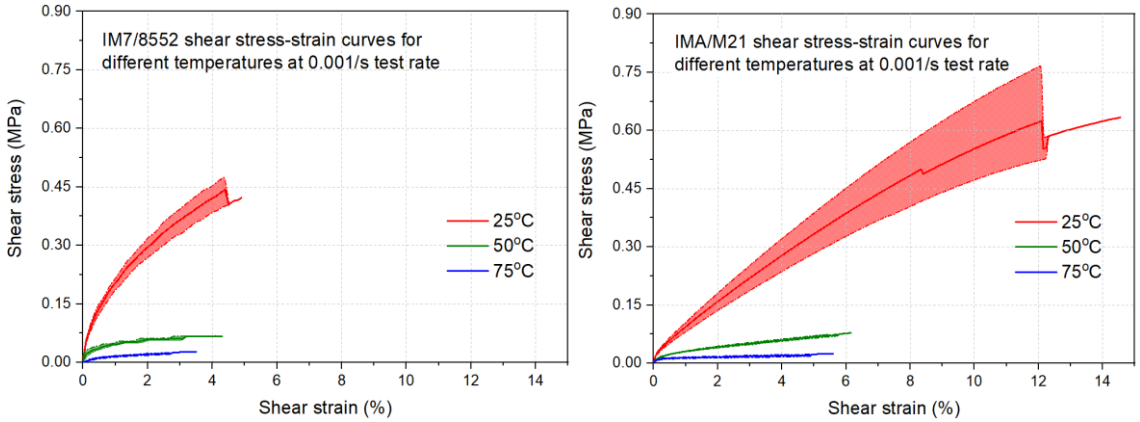

b/

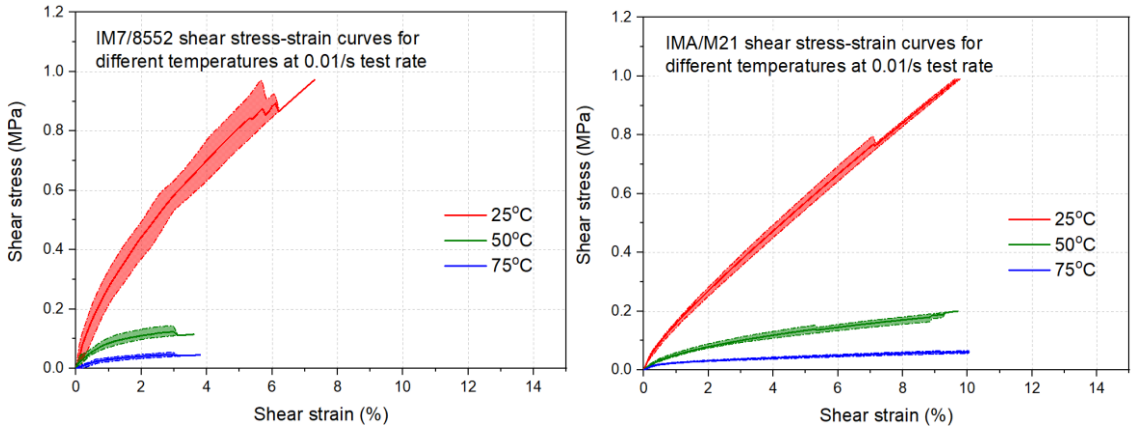

c/

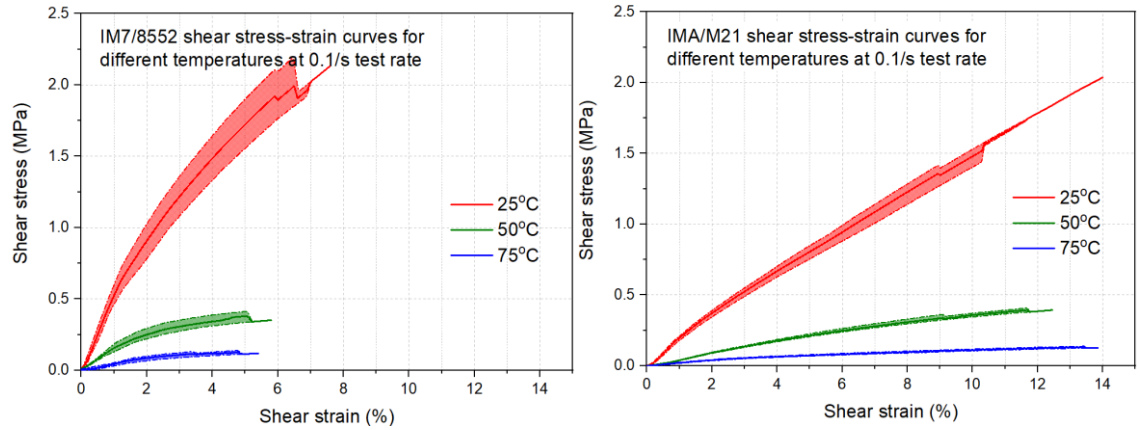

Fig. 14. Influence of temperature on the measured shear stress versus shear strain curves (left - IM7/8552 and right - IMA/M21) at test rates of a/ 0.001/s, b/ 0.01/s and c/ 0.1/s.

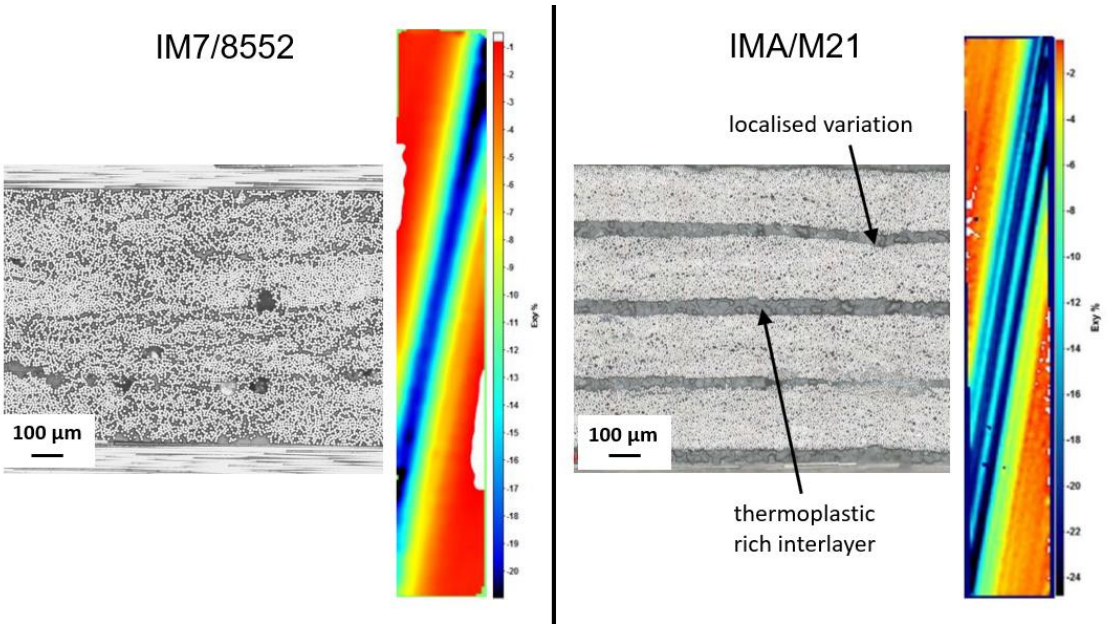

Fig. 15. Representative shear strain map obtained through DIC and meso-scale morphology for IM7/8552 (left) and IMA/M21 (right). The micrographs were taken from samples consolidated at 30ºC and then cured in an oven so as to preserve the micro-structure before sectioning [15].

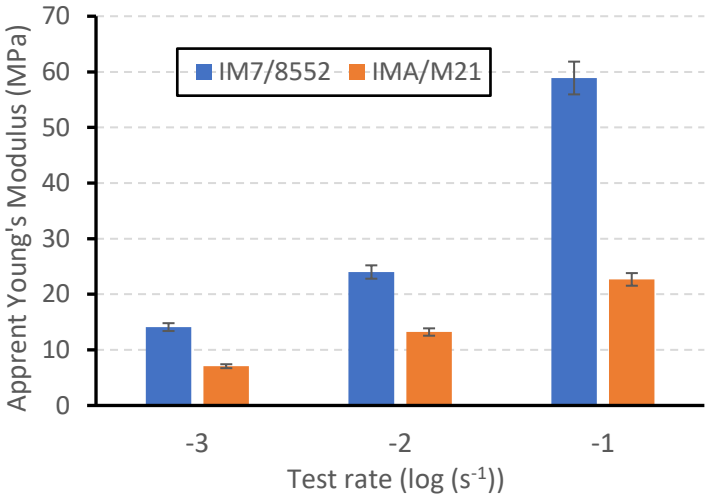

Fig. 16. The variation of the apparent Young's modulus with rate.

Tables

Table 1 Physical properties of two different toughed thermoset prepreg systems.

Different materials/Properties	Nominal fibre volume fraction	Resin content	Nominal cured ply thickness
IM7/8552	57.7%	35%	0.125 mm
IMA/M21	59.2%	34%	0.184 mm

Table 2 Test matrix for temperature influence study.

Different temperatures/Rates	**25 °C**	**50°C**	**75°C**
0.001 s^{-1}	5 repeats	5 repeats	5 repeats
0.01 s^{-1}	5 repeats	5 repeats	5 repeats
0.1 s^{-1}	5 repeats	5 repeats	5 repeats